BIO-INSPIRED FLOW SENSING AND CONTROL: AUTONOMOUS UNDERWATER NAVIGATION USING DISTRIBUTED PRESSURE MEASUREMENTS

Francis D. Lagor, Levi D. DeVries, Kathryn M. Waychoff, and Derek A. Paley
Department of Aerospace Engineering and the Institute for Systems Research
University of Maryland, College Park MD 20742
(301) 405-5757
dpaley@umd.edu

***Abstract*—This paper presents ongoing work toward the design and use of an artificial lateral-line system for a bio-inspired underwater vehicle capable of various navigation tasks enabled by flow-sensing information. We describe the results of flow-sensing and control experiments using a bio-inspired autonomous robot to achieve rheotaxis, which is the natural tendency of fish to orient upstream. We first implemented a feedback controller based on differencing pressure measurements on opposite sides of the fish robot. We also experimentally validated theoretical results for the Bayesian estimation of flow speed and angle-of-attack (orientation) by assimilating pressure measurements into a two-dimensional potential-flow model.**

I. Introduction

One challenging consideration in the design of mobile autonomous robotic systems is the influence of an unknown or unsteady flow field on vehicle motion [1],[2],[3]. However, flow fields provide rich information to the evolutionarily adaptive flow-sensing features present in some biological systems [4],[5]. The field of biomimetic flow-sensing has developed with the following objectives: (1) to use biological structures to inform the design, fabrication, and packaging of artificial flow-sensing devices for use in autonomous robotics [2],[6]; and (2) to develop algorithms for data assimilation from these complex flow-sensing arrays to achieve specific functional goals, such as local flow field estimation and object identification [7],[8],[3].

One prominent example of an advanced biological flow-sensing system is the lateral-line system present in all cartilaginous and bony fish and aquatic amphibians [8],[5]. Cartilaginous and bony fish sense local flow velocity and pressure-difference information using a lateral-line sensory system. The uses of the lateral-line system in fish include orienting in flow (rheotaxis), schooling, detecting obstacles, and avoiding predators. For example, the blind Mexican cave fish (Astyanax fasciatus) relies exclusively on the lateral-line system for orienting, navigating, and schooling [5],[4]. The lateral-line system often runs the length of the fish and is made up of receptors, known as neuromasts, ranging in number from under 100 to well over 1000 [5]. The neuromasts consist of ciliary bundles of hair cells that serve as mechano-electrical transducers with directional sensitivity covered in a gelatinous outer dome called a cupula [4]. Neuromasts exist in two types: superficial neuromasts, which are located on the exterior surface; and canal neuromasts, which are located between pore entrances of a subdermal lateral-line canal. Superficial neuromasts serve as flow velocity sensors, whereas canal neuromasts, responding to pressure-driven flow in the canal, measure pressure differences [9].

Two specific fish behaviors of interest for bio-inspired robotics are rheotaxis and station-holding. Rheotaxis is a behavior in which a fish orients upstream toward the oncoming flow; station-holding is a behavior in which a fish swims behind an upstream obstacle. Although the precise role of the lateral-line sensing modalities in executing these behaviors is not fully understood, they are thought to play an important role [4]. To this end, developing an artificial lateral-line system for use on an autonomous underwater vehicle would enhance its autonomy by providing an additional sensing modality in unknown and unsteady flows. Moreover, it would provide indispensable sensory information in dark, murky, or cluttered environments, where traditional sensing modalities like vision or sonar may be impaired.

The first artificial lateral-line was fabricated in 2006 [10]. Since then, many researchers have contributed to the field through the development of artificial lateral-line systems using a variety of sensor types, including microfabricated hot-wire anemometry [10], capacitive [11], piezoresistive [12], optical [8], and ionic polymer metal composite cantilever [7] sensors. In 2011, Yang et al. [6] designed an artificial lateral-line canal with a semi-circular cross section and subsequently demonstrated the properties of band-pass filtering and noise rejection in an artificial lateral-line using dipolar and turbulent flows. In 2012, Tao and Yu [5] provided a comprehensive review of biomimetic hair flow sensors, and Ren and Mosheni [13] performed analytical work on a model for flow

sensing of a Kármán vortex street. Abdulsadda and Tan [7] created an artificial lateral-line open to external flow, using ionic polymer metal composite cantilever sensors; they trained an artificial neural network to use features from sensor outputs to localize a nearby dipole source to within 3% error. Venturelli et al. [9] used an artificial lateral-line made of off-the-shelf piezoresistive pressure sensors (approximating the pressure-difference measurements of canal neuromasts) and showed that the array can be used to identify the presence of a Kármán vortex street, its lateral position, and hydrodynamic features.

In this paper, we specifically focus on the design and implementation of a feedback control law for rheotaxis. Although many investigators have constructed artifical lateral-lines, only a few have implemented closed-loop estimation and control using sensor data. For example, Salumäe et al. [3] demonstrated closed-loop rheotaxis of a fish robot using pressure sensors and a Braitenberg controller, and Salumäe and Kruusmaa [14] demonstrated closed-loop control station-holding of a fish robot. However, these works and others have focused on empirical methods for control. This paper describes the design and implemention of a closed-loop dynamic control framework for rheotaxis of a bio-inspired fish robot that includes model-based estimation of flow field parameters. Our technical approach employs a reduced-order fluid-mechanics model for flow past a streamlined body based on potential-flow theory. We utilize tools from Bayesian filtering to create a dynamic flow-sensing control loop for rheotaxis behavior. To validate our potential-flow model, we performed computational fluid dynamic (CFD) simulations. We constructed an experimental testbed, which consists of a 185L flow tank, a two-degree-of-freedom mechanical gantry system, and a fish robot endowed with commercially-available pressure sensors. Finally, we used this testbed to validate our dynamic controller for rheotaxis of a fish robot.

The contributions of this paper are (1) the design and fabrication of a robotic platform for testing flow estimation and control algorithms with a bio-inspired fish robot; (2) the closed-loop demonstration of rheotaxis using two pressure sensors and a proportional controller; and (3) Bayesian estimation of angle-of-attack and flow speed for flow past a fish robot, and the use of the estimated angle-of-attack in a dynamic rheotaxis controller.

The outline of the paper is as follows. Section II describes a potential-flow model for flow past a fish robot as well as a measurement equation for pressure differences in an artificial lateral-line sensor array. Section III gives an overview of recursive Bayesian filtering and presents the framework for dynamic feedback control. Section IV discusses the experimental testbed and results from a rheotaxis experiment based on a pressure-difference controller. Section V evaluates the potential-flow model against CFD simulation, presents experimental results for Bayesian estimation of a fixed angle-of-attack, and describes the performance of the Bayesian filter-based rheotaxis controller. Section VI summarizes the paper and describes our ongoing research.

II. Model for Pressure Differences in an Artificial Lateral-Line

This section presents a reduced-order fluid-mechanics model for flow past a fish body and a measurement equation to predict pressure differences between sensor locations in a bio-inspired artificial lateral-line.

A. Flow past a streamlined body

In order to make estimates of flow parameters based on sensor measurements, we invoke an idealized model of fluid flow past a streamlined airfoil. We employ potential-flow theory and conformal mapping, making use of the Joukowski transformation [15],[16]. Let $\xi = Re^{i\theta} - |\lambda|$ with $\theta \in [0, 2\pi)$ be a disk of radius R centered at λ [15]. Using the complex plane to represent the two-dimensional domain, the transformation [15]

$$z = \xi + \frac{b^2}{\xi} \in \mathbb{C}, \tag{1}$$

where $b = R - \lambda$, maps an offset disk into a symmetric streamlined body centered at the origin[1] [15]. Let $U > 0$ be the free-stream flow speed and α be the angle-of-attack of the fish relative to the flow. When transformation (1) is used in conjunction with the velocity potential [16],[15]

$$w(\xi) = U(\xi+\lambda)e^{-i\alpha} + \frac{R^2}{\xi+\lambda}Ue^{i\alpha} + 2iRU\sin(\alpha)\ln(\xi+\lambda), \tag{2}$$

it maps uniform flow past a cylindrical disk into uniform flow past a streamlined body [15],[17]. The first term in the velocity potential (2) represents uniform flow, the second term introduces the boundary condition, and the third term enforces the Kutta condition, which states that the rear stagnation point must occur at the trailing tip of the airfoil.

[1]We choose $R = 2.9$ cm and $\lambda = -.5$ cm (similar to [17]). This yields a 9.9 cm by 2.2 cm fish that approximately resembles the dimensional characteristics of a Mottled sculpin (Cottus baridi) [18],[19], a fish previously studied for rheotactic response [20].

The conjugate flow around the body in z coordinates is [15],[17]

$$f^*(z) = \frac{\partial w}{\partial \xi}\left(\frac{\partial z}{\partial \xi}\right)^{-1} = \left(Ue^{-i\alpha} - \frac{R^2}{(\xi(z)+\lambda)^2}Ue^{i\alpha} + \frac{2iRU\sin\alpha}{(\xi(z)+\lambda)}\right)\left(1 - \frac{b^2}{(\xi(z))^2}\right)^{-1}, \quad (3)$$

where * denotes complex conjugation. $\xi(z)$ is the dual-valued inverse mapping of (1) with values selected to lie outside of the fish body [15],[17], i.e.,

$$\xi(z) = \begin{cases} \frac{1}{2}\left(z + \sqrt{z^2 - 4b^2}\right), & \text{if } \arg(z) \in (-\pi/2, \pi/2] \\ \frac{1}{2}\left(z - \sqrt{z^2 - 4b^2}\right), & \text{if } \arg(z) \in (\pi/2, 3\pi/2] \end{cases}. \quad (4)$$

The real and imaginary parts of (3) give the components of the flow field. Note that the flow is evaluated at sensor placement locations and parameterized by the free-stream flow speed U and angle-of-attack α.

B. Measurement equation

A model of the pressure values predicted by the potential-flow model (3) is obtained by considering Bernoulli's principle for inviscid, incompressible flow along a streamline [21]:

$$\frac{v^2}{2} + gz + \frac{p}{\rho} = C, \quad (5)$$

where v is the local flow speed, g is the acceleration of gravity, z is the elevation, p is the static pressure, and C is a constant describing the total specific energy of a fluid parcel moving along the streamline. Applying (5) to two equal-elevation locations along a streamline, where the second location is a stagnation point, results in an expression for pressure p in terms of the streamline's stagnation pressure p_s [21]:

$$\frac{v_1^2}{2} + \frac{p_1}{\rho} = \frac{p_s}{\rho},$$

which implies (dropping the subscript 1)

$$p = p_s - \rho\frac{v^2}{2}.$$

Figure 1 illustrates two sensors on opposing sides of a fish robot. Figure 2(a) shows the ideal pressure values for various flow field parameters at one of these sensor locations with stagnation pressure $p_s = 1$ kPa. (A plot of pressure values for the opposing sensor location would be identical except mirrored about the flow speed axis.)

Figure 2(b) illustrates the difference between measurements from the two sensor locations. For an unknown angle-of-attack, the stagnation pressure p_s is not known.

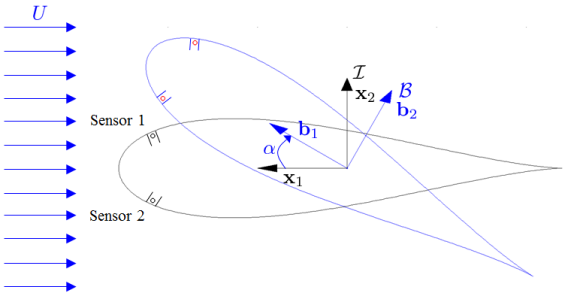

Fig. 1. Relevant reference frames and flow field parameters.

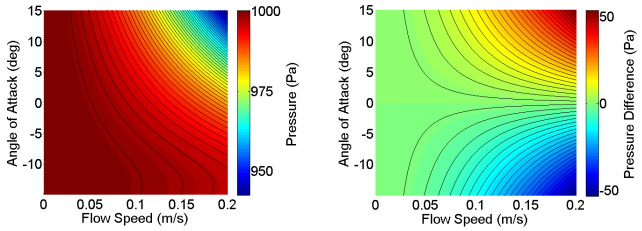

(a) (b)

Fig. 2. a) Fluid pressure at a given sensor location; b) pressure difference between two sensor locations.

However, the difference between two pressure measurements is

$$\Delta p = p_2 - p_1 = \frac{\rho}{2}\left(v_1^2 - v_2^2\right).$$

Hence, a measurement equation based on the pressure difference offers the advantage that the stagnation pressure does not need to be known. In Figure 2, the maximum value of U is chosen as 0.2 m/s to correspond to a flow speed of 2 body-lengths per second for a 10 cm fish. We limit the angle-of-attack to $\alpha \in [-15°, 15°]$ to avoid the stall condition in the study of airfoils [16],[17].

We assume that the pressure measurements contain additive white noise, i.e., the ith sensor measurement is

$$\tilde{p}_i = p_i + \eta_i, \quad (6)$$

where η_i has a zero-mean Gaussian distribution with σ_i^2 variance, $\mathcal{N}_i(0, \sigma_i^2)$. (Note the difference between sensor signals produce another random variable, $\eta_2 - \eta_1$, which has distribution $\mathcal{N}(0, \sigma_1^2 + \sigma_2^2)$.) Let $\mathbf{\Omega} = [U, \alpha]^T$. The measurement equation, after subsititution of the flow model (3) and inclusion of the measurement noise model (6), is

$$\Delta\tilde{p} = \frac{\rho}{2}\left(|f^*(z_1, \mathbf{\Omega})|^2 - |f^*(z_2, \mathbf{\Omega})|^2\right) + \eta_2 - \eta_1.$$

This equation can be used to estimate $\mathbf{\Omega}$ from pressure measurements. However, note from Figure 2(b) that U is unobservable at zero angle-of-attack (all flow speeds give $\Delta p = 0$). Similarly, α is unobservable if U is zero or if the pressure difference is smaller than the noise level of the sensors.

III. Estimation and Control Framework for Rheotaxis

This section describes a recursive Bayesian filter for estimating flow field parameters from pressure measurements and presents how the filter is integrated in a dynamic control framework for rheotaxis.

A. Bayesian estimation and filtering

Bayesian estimation is a technique by which knowledge of an unknown quantity is enhanced through the assimilation of measurements [22]. Bayes' formula is [22]

$$\underbrace{\pi(x|y)}_{\text{posterior}} \propto \underbrace{\pi(y|x)}_{\text{likelihood}} \underbrace{\pi(x)}_{\text{prior}}, \tag{7}$$

where $\pi(\cdot)$ represents a probability density function (pdf). The central idea is to use Bayes' formula (7) to adjust the prior understanding of an unknown quantity x, represented in the form of a pdf, based upon the likelihood that a measurement y was generated by a nearby state of the system. Normalization of the posterior density is required to ensure the total integral of the pdf sums to unity. (The $\propto$ symbol is used with pdf's to indicate a proportional relationship.) In practice, we perform grid-based Bayesian estimation, in which a finite volume of parameter space is discretized, and the pdf's are approximated on this grid. Normalization is performed by summing the weights of all the grid-points and dividing by the total value. The assumption of white Gaussian measurement noise results in a Gaussian likelihood function

$$\pi(\Delta\tilde{p}|\boldsymbol{z},\boldsymbol{\Omega}) \propto \exp\left(\frac{-(\Delta\tilde{p}-\Delta p(\boldsymbol{z},\boldsymbol{\Omega}))^2}{2(\sigma_1^2+\sigma_2^2)}\right).$$

(The variances σ_1^2 and σ_2^2 are chosen by collecting data from the pressure sensors and analyzing the noise statistics. Since the noise in the sensor measurements increases with free-stream flow speed, we choose σ_1^2 and σ_2^2 based on measurements at the maximum relevant flow speed.)

Pressure sensors provide a sequence of measurements represented by $\boldsymbol{D}(t-\Delta t) \triangleq \{\Delta\tilde{p}(t-\Delta t),\ldots,\Delta\tilde{p}(t_0)\}$. The posterior probability density from the previous t–Δt assimilation time is used as the prior density for assimilation at time t, yielding

$$\begin{aligned}&\pi(\boldsymbol{\Omega}(t)|\boldsymbol{D}(t)) \propto \\ &\pi\left(\Delta\tilde{p}(t)|\boldsymbol{\Omega}(t)\right)\pi\left(\boldsymbol{\Omega}(t-\Delta t)|\boldsymbol{D}(t-\Delta t)\right).\end{aligned} \tag{8}$$

The state evolution equation and the measurement equation together are an evolution-observation model, for which our knowledge of the system state can evolve in time and be augmented with new information through the following sequential, recursive scheme, known as Bayesian filtering [22]:

- Time evolution of the pdf (prediction) is accomplished using the Chapman-Kolmogorov equation [22]

$$\begin{aligned}&\pi\left(\boldsymbol{\Omega}(t+\Delta t)|D(t)\right) = \\ &\int \pi\left(\boldsymbol{\Omega}(t+\Delta t)|\boldsymbol{\Omega}(t)\right)\pi\left(\boldsymbol{\Omega}(t)|D(t)\right)d\boldsymbol{\Omega}(t).\end{aligned} \tag{9}$$

- Assimilation of the observations occurs via Bayes' formula [22]

$$\begin{aligned}&\pi\left(\boldsymbol{\Omega}(t+\Delta t)|D(t+\Delta t)\right) \propto \\ &\pi\left(D(t+\Delta t)|\boldsymbol{\Omega}(t+\Delta t)\right)\pi\left(\boldsymbol{\Omega}(t+\Delta t)|D(t)\right).\end{aligned} \tag{10}$$

In Section V-B, we choose $\pi\left(\boldsymbol{\Omega}(t+\Delta t)|\boldsymbol{\Omega}(t)\right)$ to be a Gaussian transition density, with variance chosen to improve estimator/filter performance.

B. Dynamic control design

We now present a model-based dynamic controller for rheotaxis shown in Figure 3. The kinematics of the robot turning at a commanded angular rate u are

$$\dot{\alpha} = u, \tag{11}$$

where u is the control input. The Bayesian filter produces estimates of $\hat{\alpha}$ and $\hat{U}$ as the robot moves. The estimate $\hat{\boldsymbol{\Omega}}(t)$ is the maximum a posteriori estimate of (10), i.e.,

$$\hat{\boldsymbol{\Omega}}(t) \triangleq \arg\max_{\boldsymbol{\Omega}}\ \pi\left(\boldsymbol{\Omega}(t)|D(t)\right) \tag{12}$$

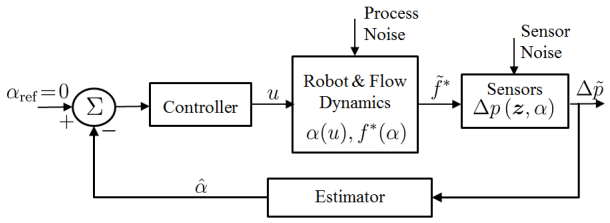

Fig. 3. Rheotaxis estimation and control framework.

The controller calculates the control input with a proportional control law given by [17]

$$u = -K_1\hat{\alpha}.$$

Since the Bayesian filter is applied in real-time, it is necessary to account for the fish motion during the estimation step. Let (11) serve as the evolution equation with process uncertainty so that the prior pdf for the next Bayesian assimilation cycle represents the best estimate of the system state. The transition density is [17]

$$\pi\left(\boldsymbol{\Omega}(t+\Delta t)|\boldsymbol{\Omega}(t)\right) = \mathcal{N}\left(\boldsymbol{\Psi},\Sigma_p\right),$$

where $\boldsymbol{\Psi} \triangleq [0\ \ \Delta t\dot{\alpha}(t)]^T$.

IV. Laboratory Testbed for Flow-sensing and Control

This section introduces the laboratory testbed constructed for experimental validation of the flow-sensing control and presents preliminary results from using this testbed to achieve autonomous rheotaxis in a bio-inspired fish robot.

A. Experimental setup

We designed and constructed a laboratory testbed consisting of a 185 L flowtank (Loligo Systems, SW10275 modified) and a two-degree-of-freedom custom robot equipped with commercially available pressure sensors, as shown in Figure 4. The flow tank has a flow straightener and 25 x 25 x 87.5 cm test section. The test section is enclosed, except for a 7 x 21 cm slot in the top for access of the robotic control arm. Calibration of the flow tank was accomplished using a Hach FH950 portable flow meter. A mechanical gantry system provides overhead control of the vehicle's orientation and cross-stream position. It is elevated by a custom 80/20 fixture and consists of an LS-100-18-H linear lead screw table (Anaheim Automation, Inc.), coupled to a secondary stepper motor for rotary motion. Both stepper motors are STM23Q-XAE integrated stepper drives (Applied Motion Products, Inc.), which take commands from LabVIEW via an RS-232 serial connection. The drives contain built-in motion controllers that accept high-level ASCII text commands, most notably feed-to-length and jog commands for control of motor position or angular velocity. The stepper motors also contain integrated encoders that can be queried directly from LabVIEW.

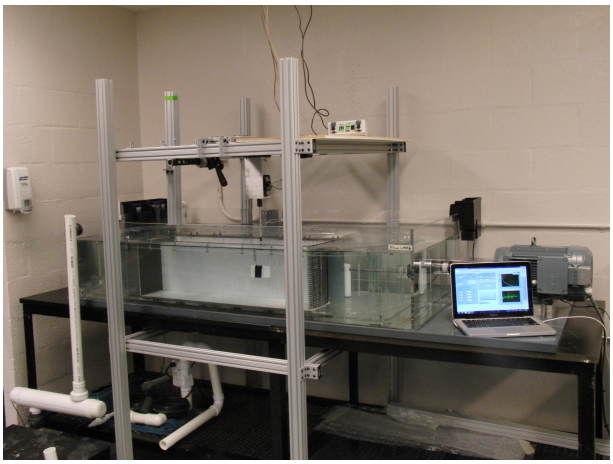

Fig. 4. The laboratory testbed consists of a 185 L flowtank and a two-degree-of-freedom underwater robot equipped with commercially available pressure sensors. The robot's overhead motors are controlled by a laptop computer.

The fish robot was constructed from a 3D-printed airfoil shape (9.9 cm long, 2.2 cm wide) when viewed from above, as seen in Figure 5. (The height of the fish was elongated to 5 cm to reduce three-dimensional effects of the flow near sensor locations.) We designed the fish in two pieces with a hollow inner pocket and port holes with small canals on opposing sides of the body for embedded pressure sensors. The sensors (Mikro-Tip Catheter Pressure Transducers) are connected to a PCU-2000 Pressure Control Unit (Millar Instruments, Inc) and embedded in canals to shield the pressure sensors from direct impingement of the fluid flow. Without the dynamic pressure contributions, the sensors read the static pressure, which enables analysis using the potential-flow model. The sensors were glued into small steel tubes within the fish robot (Figure 5(b)); wiring was fed up through the vertical rod that attaches the robot to the gantry system. A data acquisition board (National Instruments NI USB-6008) provides the link between the pressure sensors and the LabVIEW software interface.

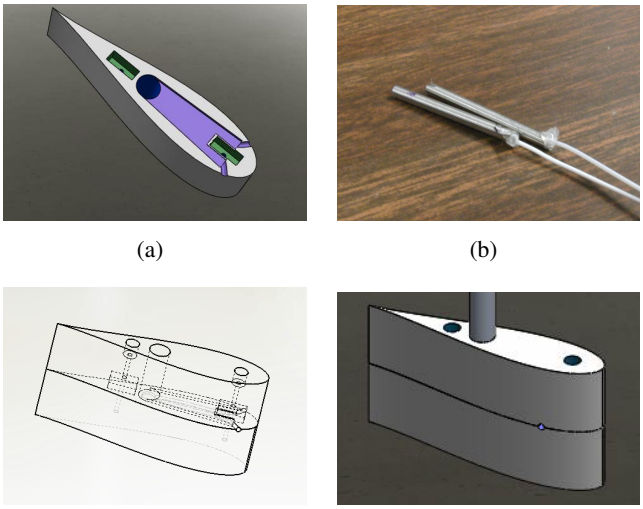

(a) (b) (c) (d)

Fig. 5. a) CAD drawing of bottom half of the fish robot; b) steel sensor isolation tubes; c) the internal features of the fish robot; d) assembled robot. Tape was applied to the seam for smoothness, except at sensor port holes.

B. Rheotaxis via pressure-difference feedback control

We implemented a feedback control for rheotaxis based on pressure differences, using signals from two pressure sensors located on opposing sides of the fish robot, as depicted in Figure 1. The control input u is calculated according to the proportional control law,

$$u = -K_2 \Delta\tilde{p} \tag{13}$$

where K_2 is a proportional gain. For initialization, pressure data is collected at zero angle-of-attack in still

water; after each run, we verify that sensor drift has not exceeded 2%, after [9]. Figure 6 shows the results of the rheotaxis experiment using (13). Note that convergence to the desired orientation is not monotonic. Further, 60 to 100 seconds elapsed before rheotaxis was achieved. It is evident that the pressure-difference signal was jagged and noisy. Although the proportional control law (13) is sufficient to accomplish rheotaxis, it lacks memory of past measurements, causing sensitivity to sensor noise.

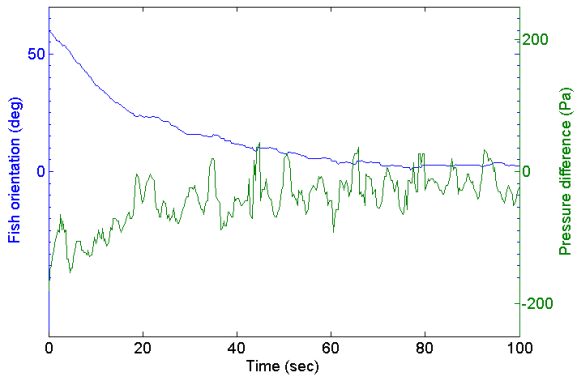

Fig. 6. Results of robotic rheotaxis using a pressure-difference feedback control.

V. Experimental Validation of Dynamic Control

This section presents results from evaluation of the potential-flow model CFD simulations and flow-tank experiments. It includes use of the potential-flow model for estimation of a fixed angle-of-attack and fixed flow speed, and presents results from using the recursive Bayesian filter for rheotaxis via a dynamic control.

A. Potential-flow model evaluation

To validate the potential-flow model from Section II, we compared it with simulations from a commercially available computational fluid dynamics solver (COMSOL) and experimental sensor data. Figures 7(a), 7(c), and 7(e) show the pressure difference between sensor locations for a constant angle-of-attack. Figures 7(b), 7(d), and 7(f) show the pressure difference for a constant free-stream flow speed. For low flow speeds and angles-of-attack, the potential-flow model accurately represents the physical phenomenon captured in the high-fidelity CFD model, with decreasing accuracy at higher flow speeds and angles. (The COMSOL CFD simulations solve the Reynolds Averaged Navier Stokes equations with a Spalart-Allmaras turbulence model [23].)
Discrepancies with experimental data are likely due to sensor noise, angular alignment uncertainty, disturbances

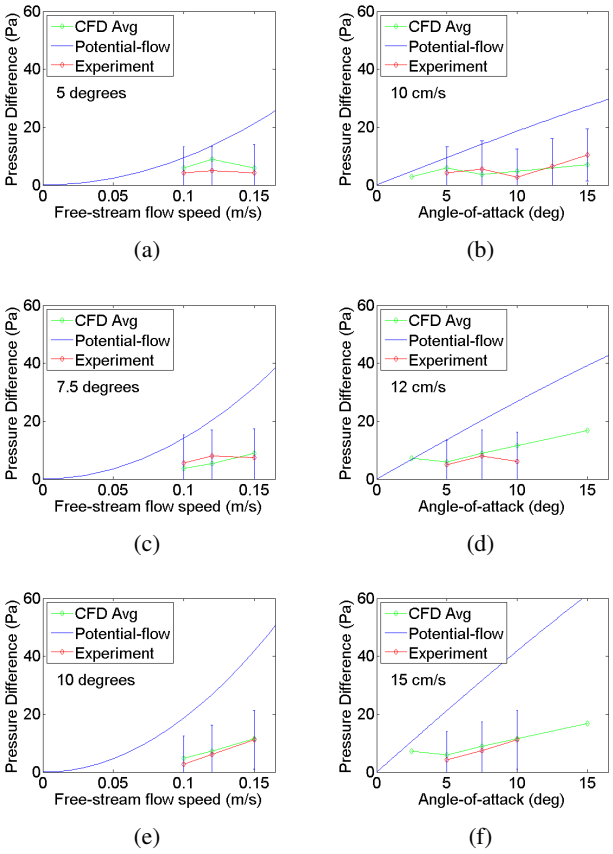

Fig. 7. a), c), and e) Comparisons for fixed angle-of-attack; b), d), and f) comparisons for fixed flow speed. Error bars represent three standard deviations from the mean.

in the free-stream flow, and unmodelled viscous effects. Nonetheless, the potential-flow model captures the general shape of the pertinent physical relationships. Additionally, the potential-flow model is a reduced-order model, offering the possibility of real-time implementation for rheotaxis control. As the closed-loop rheotaxis system converges to $\alpha = 0$, the error in the potential-flow model vanishes.

B. Static angle-of-attack and flow speed estimation

The results of Bayesian estimation for fixed angles-of-attack and flow speed experiments are shown in Figure 8. Figure 8(a) shows estimation of the true angle-of-attack to within the alignment uncertainty of the laboratory setup (approximately $\pm 2°$). Figure 8(b) illustrates how the estimator performance depends on having a small angle-of-attack; across all flow speeds, the angle-of-attack estimator performed better for 7.5°than 10°. (Note however that even the poor estimates of angle-of-attack have the correct sign.) Figure 8(c) shows the results for flow speed estimation for an angle-of-attack of 7.5°and a true flow speed of 0.17 m/s; Figure 8(d) shows a similar plot for a 10°.

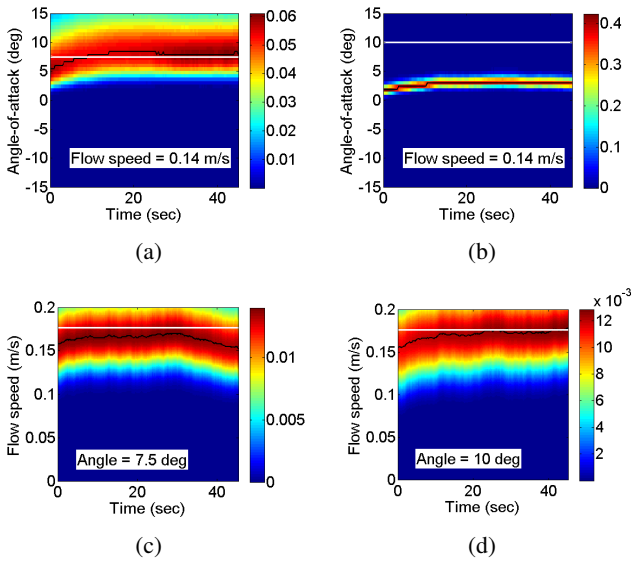

Fig. 8. Fixed angle-of-attack and flow speed estimation results. Contour plots show the marginal pdf's at each instant in time. The estimate (mode) is shown in black, and the white lines indicate the ground truth values.

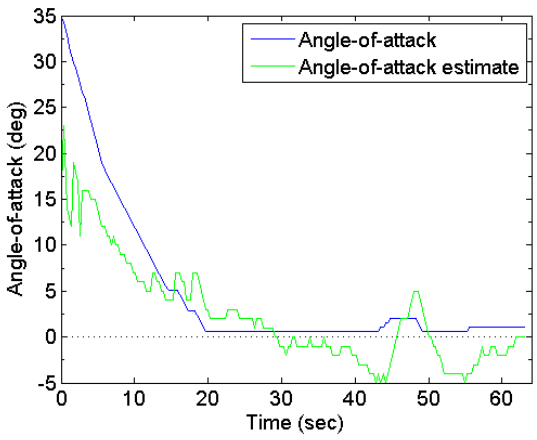

Fig. 9. Results from rheotaxis using the Bayesian filtering for dynamic feedback control.

Although the Bayesian estimation approach increases the computational work required, its benefit is reduced sensitivity to sensor noise. Figures 8(a) and 8(b) show that the estimator transient response is short (< 10 s). The estimator converges to an estimate for angle-of-attack without large excursions due to noisy data. Additionally, since the potential-flow model provides a way to predict pressure differences, the pressure sensors in principle do not need to be placed on opposing sides of the fish; the Bayesian approach allows the sensors to be placed asymmetrically, in contrast to the proportional pressure-difference controller. In the following section, we show that a dynamic controller based on the potential-flow model achieves rheotaxis from an uncertain initial orientation far outside the accurate domain of the potential-flow model.

C. Rheotaxis via dynamic control with Bayesian filtering

Results from a rheotaxis experiment using the estimation and control framework are shown in Figure 9. Although the estimates of the angle-of-attack produced by the Bayesian filter are only accurate for small angles, the control loop drives the fish robot to the upstream direction. Further, the motions of the robot are less sensitive to sensor noise during the experiment if compared to Figure 6.

VI. Conclusion

In this work, we describe closed-loop rheotaxis control of a bio-inspired fish robot. The approach employs a fluid-mechanical model for flow around a fish robot based on potential-flow theory, and provides estimates of both the fish's orientation and the free-stream flow speed. The estimation-control framework produces a dynamic controller less sensitive to sensor noise than a pressure-difference controller and was able to achieve rheotaxis from an initial orientation far outside the operational domain of the potential-flow model. In ongoing work, we are examining sensor signatures of flow behind an upstream obstacle for the development of a station-holding control law. Additionally, we will integrate flow velocity sensors with the pressure sensors used herein to produce a hybrid artificial lateral-line that more closely mimicks the two sensing modalities of a natural lateral-line system. We will use this hybrid array to improve performance on the rheotaxis task and to perform station-holding.

Acknowledgements

The authors of this work gratefully acknowledge James Tangorra and Jeff Kahn for lending us the pressure sensors used in this work and Alison Flatau and Steve Day for lending us the flow meter. The authors would also like to acknowledge valuable discussions with Sheryl Coombs, Sean Humbert, Xaiobo Tan, and Andrew Lind. This work is supported by the Office of Naval Research under Grant No. N00014-12-1-0149.

References

[1] C. Peterson and D. A. Paley, "Multivehicle coordination in an estimated time-varying flowfield," *Journal of Guidance, Control, and Dynamics*, vol. 34, no. 1, pp. 177–191, Jan. 2011.

[2] J.-M. P. Franosch, S. Sosnowski, N. K. Chami, K. Kuhnlenz, S. Hirche, and J. L. van Hemmen, "Biomimetic lateral-line system for underwater vehicles," *2010 IEEE Sensors*, pp. 2212–2217, Nov. 2010.

[3] T. Salumae and I. Ranó, "Against the flow: A Braitenberg controller for a fish robot," in *IEEE International Conference on Robotics and Automation*, 2012, pp. 4210–4215.
[4] S. Coombs, "Smart skins: information processing by lateral line flow sensors," *Autonomous Robots*, no. 1995, pp. 255–261, 2001.
[5] J. Tao and X. B. Yu, "Hair flow sensors: from bio-inspiration to bio-mimicking– a review," *Smart Materials and Structures*, vol. 21, no. 113001, pp. 1–23, Nov. 2012.
[6] Y. Yang, A. Klein, H. Bleckmann, and C. Liu, "Artificial lateral line canal for hydrodynamic detection," *Applied Physics Letters*, vol. 99, no. 2, pp. 023 701–3, 2011.
[7] A. Abdulsadda and X. Tan, "An artificial lateral line system using IPMC sensor arrays," *International Journal of Smart and Nano Materials*, vol. 3, no. 3, pp. 226–242, 2012.
[8] A. Klein and H. Bleckmann, "Determination of object position, vortex shedding frequency and flow velocity using artificial lateral line canals." *Beilstein Journal of Nanotechnology*, vol. 2, pp. 276–283, Jan. 2011.
[9] R. Venturelli, O. Akanyeti, F. Visentin, J. Ježov, L. D. Chambers, G. Toming, J. Brown, M. Kruusmaa, W. M. Megill, and P. Fiorini, "Hydrodynamic pressure sensing with an artificial lateral line in steady and unsteady flows." *Bioinspiration & Biomimetics*, vol. 7, no. 036004, pp. 1–12, Sep. 2012.
[10] Y. Yang, J. Chen, J. Engel, S. Pandya, N. Chen, C. Tucker, S. Coombs, D. L. Jones, and C. Liu, "Distant touch hydrodynamic imaging with an artificial lateral line." *Proceedings of the National Academy of Sciences of the United States of America*, vol. 103, no. 50, pp. 18 891–5, Dec. 2006.
[11] A. Dagamseh, T. Lammerink, M. Kolster, C. Bruinink, R. Wiegerink, and G. Krijnen, "Dipole-source localization using biomimetic flow-sensor arrays positioned as lateral-line system," *Sensors and Actuators A: Physical*, vol. 162, no. 2, pp. 355–360, Aug. 2010.
[12] Y. Yang, N. Nguyen, N. Chen, M. Lockwood, C. Tucker, H. Hu, H. Bleckmann, C. Liu, and D. L. Jones, "Artificial lateral line with biomimetic neuromasts to emulate fish sensing." *Bioinspiration & Biomimetics*, vol. 5, no. 16001, pp. 1–9, Mar. 2010.
[13] Z. Ren and K. Mohseni, "A model of the lateral line of fish for vortex sensing." *Bioinspiration & Biomimetics*, vol. 7, no. 036016, pp. 1–14, Sep. 2012.
[14] T. Salumäe and M. Kruusmaa, "Flow-relative control of an underwater robot," *Proceedings of the Royal Society A*, vol. 469, no. 20120671, pp. 1–19, 2013.
[15] R. L. Panton, *Incompressible flow*. New York: Wiley, 1984.
[16] J. D. Anderson, *Fundamentals of aerodynamics*. New York: McGraw-Hill, 1984.
[17] L. DeVries and D. Paley, "Observability-based optimization for flow sensing and control of an underwater vehicle in a uniform flowfield," in *American Controls Conference*, 2013, pp. 1–6.
[18] N. Beckman, "Model Systems in Neuroethology: Prey Capture in Mottled Sculpin." [Online]. Available: http://nelson.beckman.illinois.edu/courses/neuroethol/models/mottled_sculpin/mottled_sculpin.html
[19] Resources Information Standards Committee of British Columbia, "Field Key to the Freshwater Fishes of British Columbia." [Online]. Available: http://www.ilmb.gov.bc.ca/risc/pubs/aquatic/freshfish/fresht-25.htm
[20] S. Coombs, C. B. Braun, and B. Donovan, "The orienting response of Lake Michigan mottled sculpin is mediated by canal neuromasts." *The Journal of Experimental Biology*, vol. 204, no. 2, pp. 337–48, Jan. 2001.
[21] R. Fox, A. McDonald, and P. Pritchard, *Introduction to fluid mechanics*, 6th ed. Hoboken N.J.: Wiley, 2004.
[22] J. Kaipio and E. Somersalo, *Statistical and computational inverse problems*. New York: Springer, 2005.
[23] COMSOL, "The CFD module users guide," pp. 1–510, 2012.